Electronic Supplementary Material (ESI) for Journal of Materials Chemistry A.

TiO_2 Embedded Structure for Perovskite Solar Cells with Anomalous Grain Growth and Effective Electron Extraction

Dong Wei,[a] Jun Ji,[a] Dandan Song[a] Meicheng Li,[a,b*] Peng Cui,[a] Yaoyao Li,[a] Joseph Michel Mbengue, [a] Wenjia Zhou, [c] Zhijun Ning, [c] Nam-Gyu Park[d]

[a]State Key Laboratory of Alternate Electrical Power System with Renewable Energy Sources, School of Renewable Energy, North China Electric Power University, Beijing 102206, China.

[b]Chongqing Materials Research Institute, Chongqing 400707, China

[c]School of Physical Science and Technology, ShanghaiTech University, Shanghai 201210, China

[d]School of Chemical Engineering, Sungkyunkwan University, Suwon 440-746, Korea

*Corresponding author: E-mail: mcli@ncepu.edu.cn; Fax: +86 10 6177 2951; Tel: +86 10 6177 2951.

The Scanning electron microscopy (SEM) images of pristine perovskite film and the the perovskite films with different amounts of TiO_2 in TiO_2/PbI_2 blend are shown in **Fig. S1**. From the images, it is clear that the embedded TiO_2 nanoparticles can promote the growth of perovskite grains, observably. The pristine perovskite film presents the poly-crystalline morphology and the average grain size is about 100 nm. In contrast, the perovskite films embedded with TiO_2 nanoparticles (even merely 0.03 *wt*% in TiO_2/PbI_2 blend) exhibits larger grain size, along with more preferred orientation and more compact morphology.

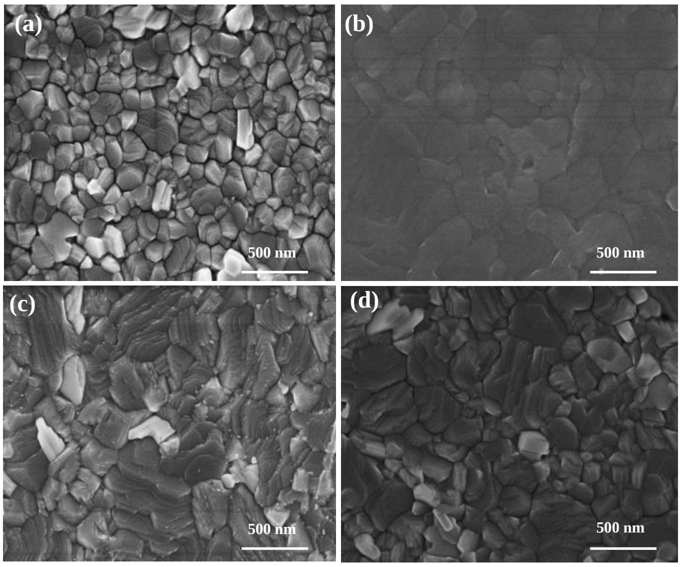

Fig. S1 (a-d) Scanning electron microscopy (SEM) images of (a) the pristine perovskite film; (b), (c) and (d) the TiO_2 embedded perovskite film (corresponding to 0.1 *wt*%, 0.05 *wt*% and 0.03 *wt*% TiO_2 in TiO_2/PbI_2 blend, respectively).

As shown in **Fig. S2**, the high-resolution transmission electron microscopy (HRTEM) image of the TiO_2 embedded perovskite is exhibited. Two different interplanar distances are presented, which are consistent to (110) planes of TiO_2 nanoparticles [1] and perovskite grains [2], respectively.

The TiO_2 nanoparticles have been embedded in the perovskite grains and have surrounded the perovskite grains. The polycrystalline perovskite grains have grain boundaries with different orientations, which can form many reentrant edges. The reentrant-edge boundaries benefit for the attachment of atoms and have much higher grain boundary energy than other boundaries, which can promote the growth of perovskite grains.

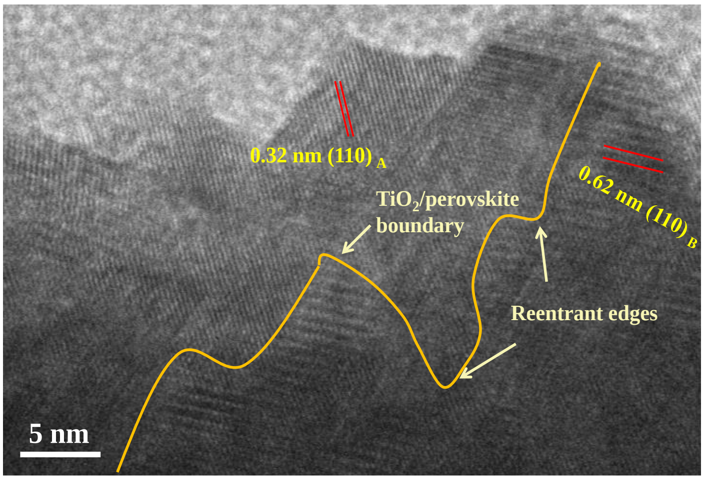

Fig. S2 High-resolution transmission electron microscopy (HRTEM) image of the TiO_2 embedded perovskite. A present TiO_2 and B present perovskite. As shown in the figure, the lattice spacing of 0.32 nm is consistent to (110) plane of rutile TiO_2 and the lattice spacing of 0.62 nm is consistent to (110) plane of perovskite. The reentrant-edge boundaries benefitting for the grain growth, are also exhibited.

The schematic diagrams of the four different process of the time resolved photoluminescence spectroscopy (TRPL) measurement are given in **Fig. S3**. For comparison, the perovskite film on compact TiO_2 is measured from the TiO_2 side and the perovskite side, respectively, and show in figure (a); the pristine perovskite film and the TiO_2 embedded perovskite film are also characterized as shown in figure (b) and figure (c). When under irradiation, there will be many photo-induced carriers. These carriers can be extracted and transport by TiO_2 or be recombined by traps and other carriers.

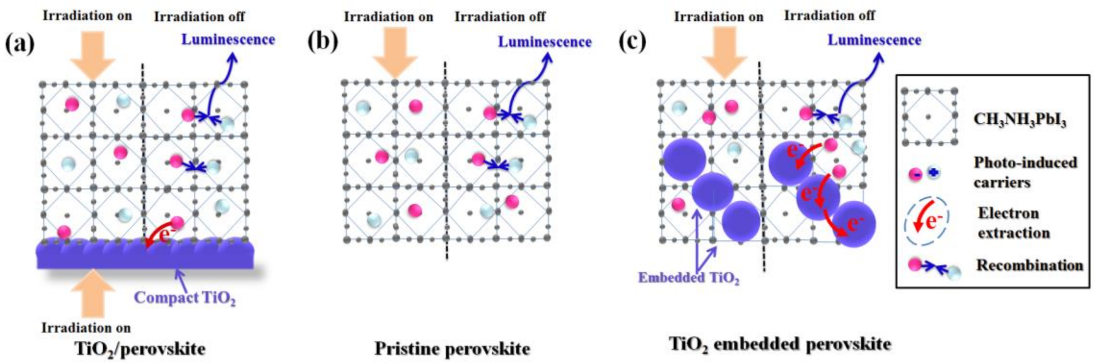

Fig. S3 Schematic illustrating of the electron extraction and electron transport properties of the perovskite films during the time resolved photoluminescence spectroscopy (TRPL) measurement: (a) TiO_2/perovskite film, which was irradiated from the perovskite side and the compact TiO_2 side, respectively. (b) Pristine perovskite film and (c) embedded perovskite film, which were irradiated from the perovskite side.

As shown in **Fig. S4**, the high-resolution transmission electron microscopy (HRTEM) image and the Scanning transmission electron microscopy (STEM) images of the embedded perovskite are displayed. From Fig. S4 (d), it can be observed clearly that the iodine elements are surrounded by titanium, indicating that the embedded TiO_2 nanoparticles present in the boundaries of perovskite grains. Moreover, these embedded TiO_2 is distributed continuously, forming a passage for transporting the electrons extracted from perovskite, as shown in Fig. S4 (c).

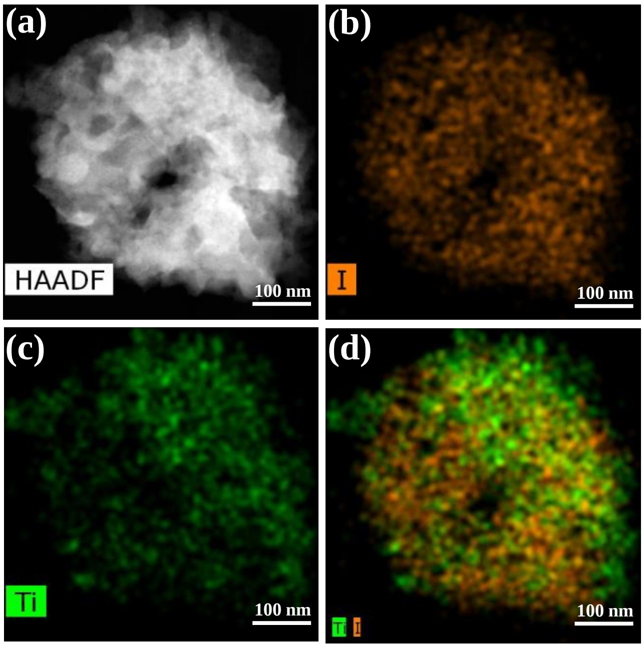

Fig. S4 (a) High-resolution transmission electron microscopy (HRTEM) image of TiO_2 embedded perovskite. (b) Scanning transmission electron microscopy (STEM) image of iodine elements. (c) STEM image of titanium elements and (d) STEM image of the iodine and titanium elements of the embedded perovskite grain.

The cross-section SEM images of the standard planar PSC and the TiO_2 embedded PSC were shown in **Fig. S5**. Compared to the cross-section SEM of the standard planar PSC, it can be observed clearly that the cross-section SEM of embedded perovskite film demonstrates that the embedded TiO_2 nanoparticles form many electron transport paths, which can conduct the electrons from the perovskite layer to the compact TiO_2 layer. Hence, it can be concluded that the electrons injected from perovskite to TiO_2 nanoparticles can be transported through the continuous TiO_2 nanoparticle network and collected by the compact TiO_2 layer.

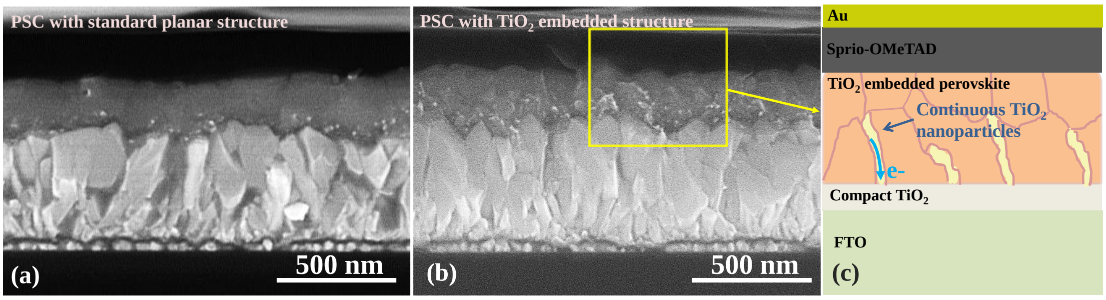

Fig. S5 Cross-section SEM figures of the PSC with the standard planar structure and with the TiO_2 embedded structure. The schematic illustrating the structure of the TiO_2 embedded perovskite solar cells and the networks of the embedded TiO_2.

As shown in **Fig. S6**, the high-resolution transmission electron microscopy (HRTEM) image and the scanning transmission electron microscopy coupled with energy dispersive X-ray spectroscopy (STEM-EDS) of TiO_2 embedded perovskite grains are exhibited. From these figures, it is able to see that many perovskite grains stack with each other grains, and the TiO_2 nanoparticles are embedded in the boundaries of perovskite grains.

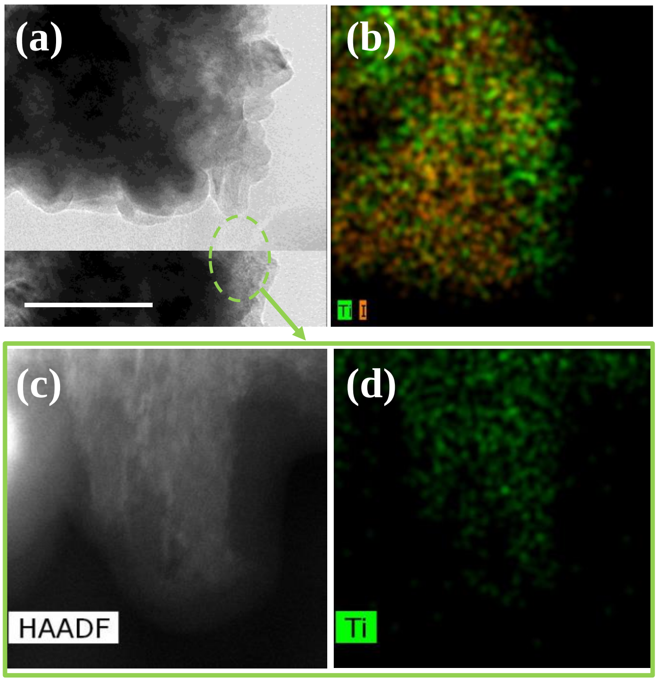

Fig. S6 (a) High-resolution transmission electron microscopy (HRTEM) image and (b) scanning transmission electron microscopy coupled with energy dispersive X-ray spectroscopy (STEM-EDS) of TiO_2 embedded perovskite. (c) High-angle annular dark-field scanning transmission electron microscopy (HAADF-STEM) and (d) STEM-EDS of the embedded TiO_2.

To characterize the chemical change of the perovskite films upon degradation, the X-ray diffraction (XRD) measurement was employed, as shown in **Fig. S7** (a, b). In the fresh perovskite films, a series of diffraction peaks can be observed, which can be indexed to the typical diffraction peaks of perovskite and FTO. In the degraded perovskite film, an additional diffraction peak locating at 12.6 °can be observed [3], which can be indexed to the (001) plane of PbI_2, proving that partial of the perovskite is decomposed to PbI_2. It is clear that the TiO_2 embedded perovskite film shows better stability in the ambient air.

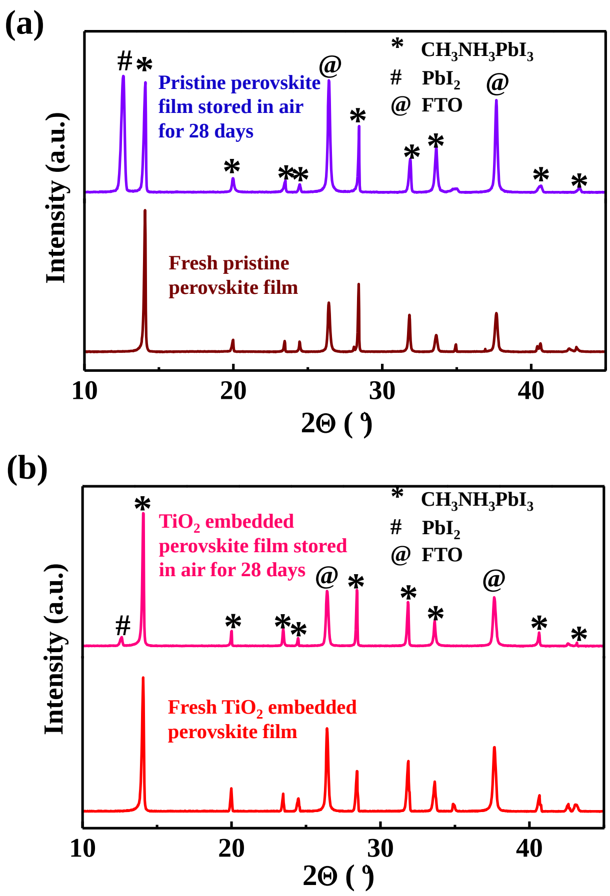

Fig. S7 XRD patterns of the pristine perovskite film (a) and the TiO_2 embedded perovskite film (b) before and after being stored in ambient air for 28 days.

As shown in **Fig. S8**, XRD pattern and TEM image of the embedded TiO_2 nanoparticle is exhibited. From the XRD pattern, it is clear that the embedded TiO_2 belonging to rutile phase (PDF NO. 21-1276) is well crystallized. From the TEM image, it can be observed clearly that the lattice spacing of 0.32 nm is consistent to (110) plane of rutile TiO_2.

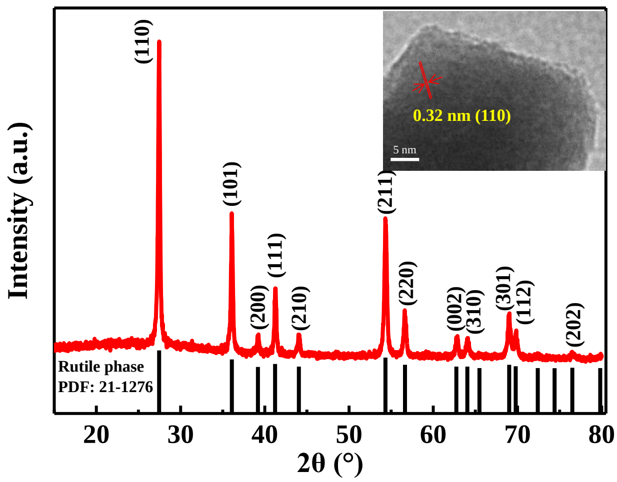

Fig. S8 XRD pattern of TiO_2 nanoparticles using into the TiO_2 embedded PSCs and TEM image (inside figure) of TiO_2 nanoparticles embedded into the perovskite films.

Reference:

1 N. Witit-anun, P. Rakkwamsuk, P. Limsuwan, Characterization of Anatase and Rutile TiO_2 Thin Films Deposited by Two Cathodes Sputtering System, *Adv. Mater. Res.*, 2008, **55-57**, 469-472.

2 M. shirayama, M. Kato, T. Miyadera, T. Sugita, T. Fujiseki, S. Hara, H. Kadowaki, D. Murata, M. Chikamatsu, H. Fujiwara, Degradation mechanism of $CH_3NH_3PbI_3$ perovskite materials upon exposure to humid air, *J. Appl. Phys.*, 2016, **119**, 115501.

3 C. Roldan-Carmona, , P. Gratia, , I. Zimmermann, G. Grancini, , P. Gao, M. Graetzel, M. K. Nazeeruddin, High efficiency methylammonium lead triiodide perovskite solar cells: the relevance of non-stoichiometric precursors, *Energ. Environ. Sci.*, 2015, **8**, 3550-3556.